Astron. Astrophys. 350, 827–839 (1999)

ASTRONOMY AND ASTROPHYSICS

On star formation and chemical evolution in the Galactic disc

L. Portinari and C. Chiosi

Department of Astronomy, University of Padova, Vicolo dell'Osservatorio 5, 35122 Padova, Italy (portinari, chiosi@pd.astro.it)

Received 10 June 1999 / Accepted 26 August 1999

Abstract. The abundance gradients and the radial gas profile of the Galactic disc are analysed by means of a model for the chemical evolution of galaxies. As one of the major uncertainties in models for galaxy evolution is the star formation (SF) process, various SF laws are considered, to assess the response of model predictions to the different assumptions. Only some SF laws are successful in reproducing the metallicity gradient, and only if combined with a suitable infall timescale increasing outward (inside–out formation scenario). Still, it is difficult to reproduce at the same time also the observed gas distribution; we therefore suggest further improvements for the models.

Key words: Galaxy: stellar content – Galaxy: evolution – Galaxy: abundances

1. Introduction

Modelling and understanding the formation and evolution of galaxies is a major issue of modern astrophysics, involving a variety of approaches: dynamical and hydro-dynamical simulations, chemical evolution models, stellar population synthesis techniques. Any galaxy model requires a recipe for the star formation (SF) process, which unfortunately is still poorly known, especially on the large scales relevant to galaxy evolution. A variety of SF laws has been suggested in literature especially for spiral galaxies, where we can observe on–going SF on large scales. In chemical models for galactic discs, different prescriptions for the SF process are used by different authors. This is true also for models of the disc of the Milky Way, a system which we can observe and study in much closer detail than any other. It is often hard to compare models and conclusions by different authors, since it is not clear to what extent model results have a general validity or rather depend on differing assumptions for the SF law.

The present work is addressed at testing different prescriptions for the SF law in the Galactic disc. To this aim we use a model for the chemical evolution of galaxies, able to handle different options for the SF law (Sect. 2). We review existing data on the abundance gradients and on the radial gas and star formation rate (SFR) profiles of the Galactic disc (Sect. 3). To these observational counterparts we compare models with the various SF laws, trying to discriminate, if possible, a "best–fit" law (Sect. 4). Summary and conclusions are finally drawn in Sect. 5.

A similar analysis was already performed by Prantzos & Aubert (1995), but an upgrade of their study is suggested since some basic observational results have meanwhile changed, especially regarding the metallicity gradient (Sect. 3).

2. The chemical model and the SF laws

The chemical evolution of the Galactic disc is simulated by means of the model of Portinari et al. (1998, hereinafter PCB98), to which we refer for a detailed description. Here we just overview the main features of the model.

It is an open model with continuous infall, as suggested by the metallicity distribution of G–dwarfs in the Solar Vicinity (Lynden-Bell 1975) and by dynamical simulations of disc formation (e.g. Larson 1976). Open models also seem to be appropriate for galaxies more in general — for instance, see Bressan et al. (1994) for the analogous of the G–dwarf problem in elliptical galaxies. The infalling gas, assumed to be primordial, settles onto the disc at an exponentially decreasing rate with timescale $\tau(r)$:

$$\dot{\sigma}_{inf}(r,t) = A(r)\, e^{-\frac{t}{\tau(r)}}$$

$A(r)$ is fixed by the assigned final (present–day) surface density profile of the model disc, an exponential with scale–legth r_d:

$$\sigma(r,t_G) = \sigma_\odot\, e^{-\frac{r-r_\odot}{r_d}}$$

where $\sigma_\odot = \sigma(r_\odot, t_G)$, total surface density at the Solar radius at the final Galactic age t_G.

In PCB98 the chemical model was applied only to the Solar Neighbourhood, while in the present paper several concentric cylindrical shells (rings) are calculated, spanning the Galactic disc from 2 to 20 kpc. Each ring, typically 2 kpc wide, consists of a homogenous mixture of gas and stars which is assumed to evolve independently, neglecting any possible radial flows. The instantaneous recycling approximation (IRA) is relaxed in the calculation of stellar ejecta. The chemical evolution of the

Send offprint requests to: L. Portinari

interstellar medium (ISM) in each ring r is described by the set of equations:

$$\begin{aligned}\frac{d}{dt}G_i(r,t) = & -X_i(r,t)\,\Psi(r,t) + \\ & + \int_{M_l}^{M_u} \Psi(r,t-\tau_M)\,R_i(M)\,\Phi(M)\,dM + \\ & + \left[\frac{d}{dt}G_i(r,t)\right]_{inf}\end{aligned} \quad (1)$$

where the G_i's are the surface gas densities of each chemical species i, normalized to the total surface density at the present age of the Galaxy $\sigma(r,t_G)$. The first term on the right-hand side represents the depletion of species i from the gaseous phase due to SF; the second term is the amount of species i ejected back to the ISM by dying stars; the third term is the contribution of the infalling gas.

The various ingredients of Eq. (1) and its numerical solution are described in detail in PCB98. With respect to that model, the only difference is that here we adopt different options for the SFR, $\Psi(r,t)$. We describe here below the various SF laws considered, together with their physical underpinnings.

2.1. Schmidt law

A few analytical prescriptions for the SF law in galactic discs are available in literature. The easiest physical law is Schmidt (1959) law:

$$SFR \propto \sigma_g^\kappa$$

where σ_g is the surface gas density. In spite of its crudeness, Schmidt law still remains, after 40 years, the most popular SF law in galaxy models.

Recent empirical determinations in spiral and starburst galaxies indicate a "Schmidt exponent" $\kappa \sim 1.5$ (Kennicutt 1998). The observed correlation is quite good between the SFR and the total density of cold gas (HI+H_2), while no clear correlation apparently holds between the SFR and the sole H_2 component — at odds with expectations since stars form within molecular clouds. Therefore, we consider here a Schmidt law with exponent 1.5, involving the overall gas density with no distinction between the atomic and the molecular phase.

In the formalism of our model, we translate Schmidt law into a normalized SFR per unit surface density (the function Ψ in Eq. 1) as:

$$\Psi(r,t) = -\left[\frac{dG}{dt}\right]_*(r,t) = \nu\left[\frac{\sigma(r,t_G)}{\sigma(r_\odot,t_G)}\right]^{\kappa-1} G^\kappa(r,t) \quad (2)$$

where we have introduced the constant normalization factor $\sigma(r_\odot,t_G)^{-(\kappa-1)}$ for the sake of expressing the SF efficiency ν in $[t^{-1}]$. We adopt $\kappa = 1.5$.

Hereinafter, chemical models adopting the Schmidt law (2) will be labelled with S15.

Other SF laws still assume that the SFR depends on the gas density, but also take into account additional phenomena affecting the SF process. As a result, the efficiency with which the available gas is turned to stars depends on the galactocentric distance r. Such laws can be written as "modified" Schmidt laws, with a proportionality coefficient, or efficiency, varying radially over the disc:

$$SFR = \nu(r)\,\sigma_g^\kappa$$

The detailed radial behaviour is related to the physical processes involved, as we discuss in the following cases.

2.2. Spiral density waves trigger

According to a theory dating back to Roberts (1969) and Shu et al. (1972), SF takes place in spiral arms due to gas compression in density waves. In this framework, Oort (1974) suggested that the SFR at a given galactocentric distance is determined by the rate at which the orbiting gas crosses spiral arms:

$$SFR \propto (\Omega(r) - \Omega_p)\,\sigma_g^\kappa$$

where $\Omega(r)$ is the angular rotation velocity as a function of radius and Ω_p is the angular velocity of the spiral pattern. In the scenario for disc galaxy formation within a pre-existing dark halo, and also according to viscous disc models (e.g. Saio & Yoshii 1990), the rotation curve is time–independent and keeps the same shape throughout the evolution. For a flat rotation curve typical of galactic discs $\Omega(r) \propto r^{-1}$, and since usually $\Omega_p \ll \Omega(r)$, we roughly get:

$$SFR \propto r^{-1}\,\sigma_g^\kappa$$

Such a SF law was adopted, for instance, by Wyse & Silk (1989) and by Prantzos & Silk (1998).

A similar radial dependence of the SF efficiency was also obtained by Wang & Silk (1994), who treated the SF process as a consequence of gravitational instabilities in the disc. These are related to the local Toomre's stability parameter Q, itself related to the local epyciclic frequency

$$\kappa_e(r) \propto \Omega(r) \propto r^{-1}$$

Normalizing the expression so that the efficiency coefficient ν is in units of $[t^{-1}]$, in our chemical model we express this "Oort SF law" as:

$$\Psi(r,t) = \nu\left[\frac{r}{r_\odot}\right]^{-1}\left[\frac{\sigma(r,t_G)}{\sigma(r_\odot,t_G)}\right]^{\kappa-1} G^\kappa(r,t) \quad (3)$$

Kennicutt (1998) noticed that his empirical relation between the current SFR and the gas surface density, yielding $\kappa \sim 1.5$ if fitted with a Schmidt law, is equally well fitted with an Oort–type law with $\kappa = 1$. Therefore, in the Oort SF law (3) we will adopt an exponent $\kappa = 1.0$. Such models will be labelled hereinafter with O10.

For the sake of comparison with other authors, we will though consider also the case of an Oort–type law with $\kappa = 1.5$ (models O15, see Sect. 4.4).

2.3. Self-regulating gravitational settling + feed-back

Other prescriptions describe SF as a self-regulation process between the gravitational settling of the gas onto the plane of the

disc and the energy feed-back from massive stars. The former phenomenon leads to compression and cooling of the gas layer, favouring its collapse into clouds and stars. Stellar winds and supernova explosions from massive stars provide a heating and turbulence source that supports the gas layer against further compression and cooling. The SFR results from the balance between these two opposing effects. Where the total surface mass density σ is larger, gravitational settling and the related cooling are more efficient, and a larger SFR is required to reach the equilibrium feed-back. As a result, the SFR depends both on the gas surface density σ_g and on σ. Since in spiral discs σ displays an exponential profile, the SF efficiency inherits an exponential radial decline. Such a self-regulating SF process was first proposed by Talbot & Arnett (1975) as:

$$SFR \propto \sigma(r)^{\kappa-1}\,\sigma_g^{\kappa} \tag{4}$$

A similar formulation was suggested later by Dopita (1985). Self-regulating SFRs depending on the local surface mass density are also obtained in full chemo-dynamical models (Burkert et al. 1992).

More recently, Dopita & Ryder (1994) discovered that an empirical relation holds in spiral discs between the H_α emission, tracing on–going SF, and the surface I–band brightness, tracing the underlying old stellar component and thus the total surface density. This relation provides the observational counterpart to a SFR depending on σ. Dopita & Ryder derived a theoretical SF law (strongly reminiscent of the one by Talbot & Arnett):

$$SFR \propto \sigma^n\,\sigma_g^m \tag{5}$$

with $n = 1/3$, $m = 5/3$, which fits very well with the observed relation. It can also account for the observed correlation between oxygen abundance and surface brightness in spiral discs (Ryder 1995).

In the formalism of our chemical model, normalizing the SFR (5) so that the efficiency coefficient ν is always in units of $[t^{-1}]$, we write:

$$\Psi(r,t) = \nu\left[\frac{\sigma^n(r,t)\,\sigma^{m-1}(r,t_G)}{\sigma(r_\odot,t_G)^{n+m-1}}\right] G^m(r,t) \tag{6}$$

and we adopt $n = 1/3$, $m = 5/3$. Chemical models with this SF law will be labelled with DR.

In PCB98 the SF law by Talbot & Arnett (Eq. 4) was adopted. That SF law, with Schmidt–like exponent $\kappa = 1.5$, naturally leads to similar predictions as models DR, since the two SF laws are analogous. Therefore, it's not worth in the following discussion to present also models with Talbot & Arnett's law separately.

2.4. The initial mass function

Besides the infall timescale $\tau(r)$ and the SF efficiency ν of the various SF laws, another important model parameter is related to the Initial Mass Function (IMF). We adopt a power–law IMF:

$$\Phi(M) \propto M^{-\mu}$$

where μ=1.35 for $M < 2\,M_\odot$ as in Salpeter (1955) and μ=1.7 for $M > 2\,M_\odot$ following Scalo (1986). Since the bulk of chemical enrichment is due to stars with $M \geq 1\,M_\odot$, a meaningful parameter is the fraction ζ of the total stellar mass distributed in stars above 1 $M_\odot$.

$$\zeta = \int_1^{100} \Phi(M)\,dM$$

Fixing the "scaling fraction" ζ is equivalent to fixing the lower end M_l of the IMF (see PCB98 and Chiosi & Matteucci 1982 for further details). In our models we always keep the IMF constant all over the disc and in time.

3. Observational constraints

In this section we review the available observational data on the abundance gradients and on the gas and SFR radial profiles in the Galactic disc. In the next section we will discuss how predictions from chemical models, adopting the different SF laws, compare to these observational data.

3.1. Metallicity gradients

Negative radial gradients of metallicity in spiral discs have long been established. Abundance data are usually derived from HII regions and from bright blue stars. These young objects mainly trace the present-day gradient for oxygen, and then for nitrogen, sulfur, neon and argon. For the Milky Way, the first extensive study of abundances in HII regions was presented by Shaver et al. (1983). Later studies based on optical spectra, in the inner and outer Galaxy, are by Fich & Silkey (1991) and Vilchez & Esteban (1996). Abundances in HII regions have been also measured from FIR lines (Simpson et al. 1995, Afflerbach et al. 1997, Rudolph et al. 1997). Studies on HII regions generally agree on the existence of a Galactic oxygen gradient around –0.07 dex/kpc. Maciel & Köppen (1994) used Type II planetary nebulæ as tracers of the present-day gradient, which they derive to be –0.06 dex/kpc, consistently with studies on HII regions.

At odds with nebular studies, the stellar spectra of OB stars and associations seemed to suggest a very flat oxygen gradient (Gehren et al. 1985; Fitzsimmons et al. 1990, 1992; Kaufer et al. 1994; Kilian-Montenbruck et al. 1994). The discrepancy disappears in the recent, extensive studies by Smartt & Rolleston (1997) and by Gummersbach et al. (1998), both deriving a gradient of –0.07 dex/kpc. This revision of the oxygen gradient in our Galaxy, in fact, suggested to us to revise as well the study by Prantzos & Aubert (1995) on the SF and chemical evolution of the Galactic disc.

In spite of the overall agreement, it is still controversial whether the slope of the oxygen gradient is constant all over the disc or not. A flattening in the outer zones has been claimed by Vilchez & Esteban (1996) and Fich & Silkey (1991), while other studies do not suggest such a trend (Smartt & Rolleston 1997; Rudolph et al. 1997; Afflerbach et al. 1997). In the overall, considering all the different data and tracers together (Fig. 1), we

Table 1. Observed abundance gradients of various elements. Δr is the galactocentric radial range covered by each respective study (in kpc). Gradients are expressed in dex/kpc.

tracer	reference	Δr	$\frac{d[O/H]}{dr}$	$\frac{d[N/H]}{dr}$	$\frac{d[S/H]}{dr}$
HII regions	Shaver et al. (1983)[(1)]	4–13	-0.07±0.015	-0.09±0.015	-0.01±0.02
(optical)	Fich & Silkey (1991)	12–18	—	~ 0	—
	Vilchez & Esteban (1996)	12–18	-0.036±0.02	-0.009±0.020	-0.041±0.020
HII regions	Rudolph et al. (1997)[(2)]	0–17	-0.079±0.009	-0.111±0.012	-0.079±-0.009
(FIR)	Afflerbach et al. (1997)	0–12	-0.064±0.009	-0.072±0.006	-0.063±0.006
OB stars	Smartt & Rolleston (1997)	6–18	-0.07±0.01	—	—
	Gummersbach et al. (1998)	5–14	-0.07±0.02	-0.08±0.02	—
Type II PNæ	Maciel & Köppen (1994)	4–14	-0.06±0.01	—	-0.07±0.01

(1) Rescaled to $r_\odot = 8.5$ kpc.
(2) Includes the data of Simpson et al. (1995).

consider that a single–slope gradient is a good enough description, and take

$$\frac{d[O/H]}{dr} = -0.06 \div -0.07 \,\mathrm{dex\,kpc^{-1}}$$

as our estimate of the oxygen gradient throughout the Galactic disc.

A similar controversy also exists for the [N/H] gradient (Fig 3, top panel) which flattens out according to optical studies (Shaver et al. 1983; Fich & Silkey 1991; Vilchez & Esteban 1996), while it remains roughly constant according to FIR measurements (Simpson et al. 1995; Rudolph et al. 1997; Afflerbach et al. 1997). The problem seems to arise from the very different, by 0.3–0.4 dex, nitrogen abundance determinations around $r \sim r_\odot$ in the two sets of analysis (Rudolph et al. 1997).

The very flat gradient of sulfur found by Shaver et al. (1983) is not confirmed in later studies; the sulfur gradient (Fig. 3, middle panel) seems rather to follow the oxygen gradient, or equivalently the [S/O] ratio seems to be constant with radius, as expected for an abundance ratio of two primary elements produced by the same source (type II SNæ). There seems to be no longer need to account for a gradient in the [S/O] ratio by invoking slightly different progenitors for the two elements, like SNæ from massive stars of different mass ranges (Matteucci & François 1989).

The abundance gradients as determined in the above mentioned studies are listed in Table 1; the corresponding data are displayed in Fig. 1. For the sake of completeness, from the above mentioned studies we plot also the data concerning the Galactic Centre. However, we will not consider these data as a constraint for chemical models of the disc, since the stellar population of the Galactic Centre is likely to have evolved on its own, rather than represent an extension of the disc population to $r \to 0$. Our disc models will consider only regions down to about $r = 2$ kpc, as further inward the Bulge becomes the dominating Galactic component.

The radial gradient of [Fe/H] is mainly traced by open clusters. An up-to-date determination based on a homogeneous sample of open clusters can be found in Carraro et al. (1998), who find

$$\frac{d[Fe/H]}{dr} \sim -0.07 \div -0.09 \,\mathrm{dex\,kpc^{-1}}$$

in good agreement with previous results (Janes 1979; Friel 1995).

3.2. Gas and SFR radial profiles

The radial profile of the cold gas distribution (sum of HI and H_2) is taken from the review by Dame (1993; Fig. 4, top panel). For $r > 7$ kpc, the profile is shallow with a plateau or a mild decline outward, while around 4–7 kpc a pronounced peak is due to the molecular ring. For $r < 3$ kpc, there is a rapid drop in the gas density.

Estimates for the SFR over the disc come from the distribution of SN remnants (Guibert et al. 1978), of pulsars (Lyne et al. 1985), of Lyman–continuum photons (Güsten & Mezger 1982) and of molecular gas (Rana 1991 and references therein). Following Lacey & Fall (1985), since these observables cannot directly yield the absolute SFR without assumptions on the IMF etc., we just normalize them to their value at the Solar ring, and consider them as tracers of the radial profile SFR(r)/SFR($r_\odot$) (Fig. 4, bottom panel). Unsurprisingly, the observed SFR profile follows that of the gas distribution, with a peak around $r = 4$ kpc.

4. Model results

In this section we compare model results for the various SF laws to the observed radial profile of the disc.

The models are calibrated as follows. The age of the Galaxy is t_G=15 Gyr. The final density profile of the disc $\sigma(r, t_G)$ is exponential with scale-length r_d and with a surface mass density at the Solar ring ($r_\odot = 8.5$ kpc) of $\sigma(r_\odot, t_G) = 50\ M_\odot$ pc^{-2} (PCB98 and references therein). In most models, $r_d = 4$ kpc and the infall timescale at the Solar ring is $\tau(r_\odot) = 3$ Gyr; different values for the infall timescale at the Solar ring and for

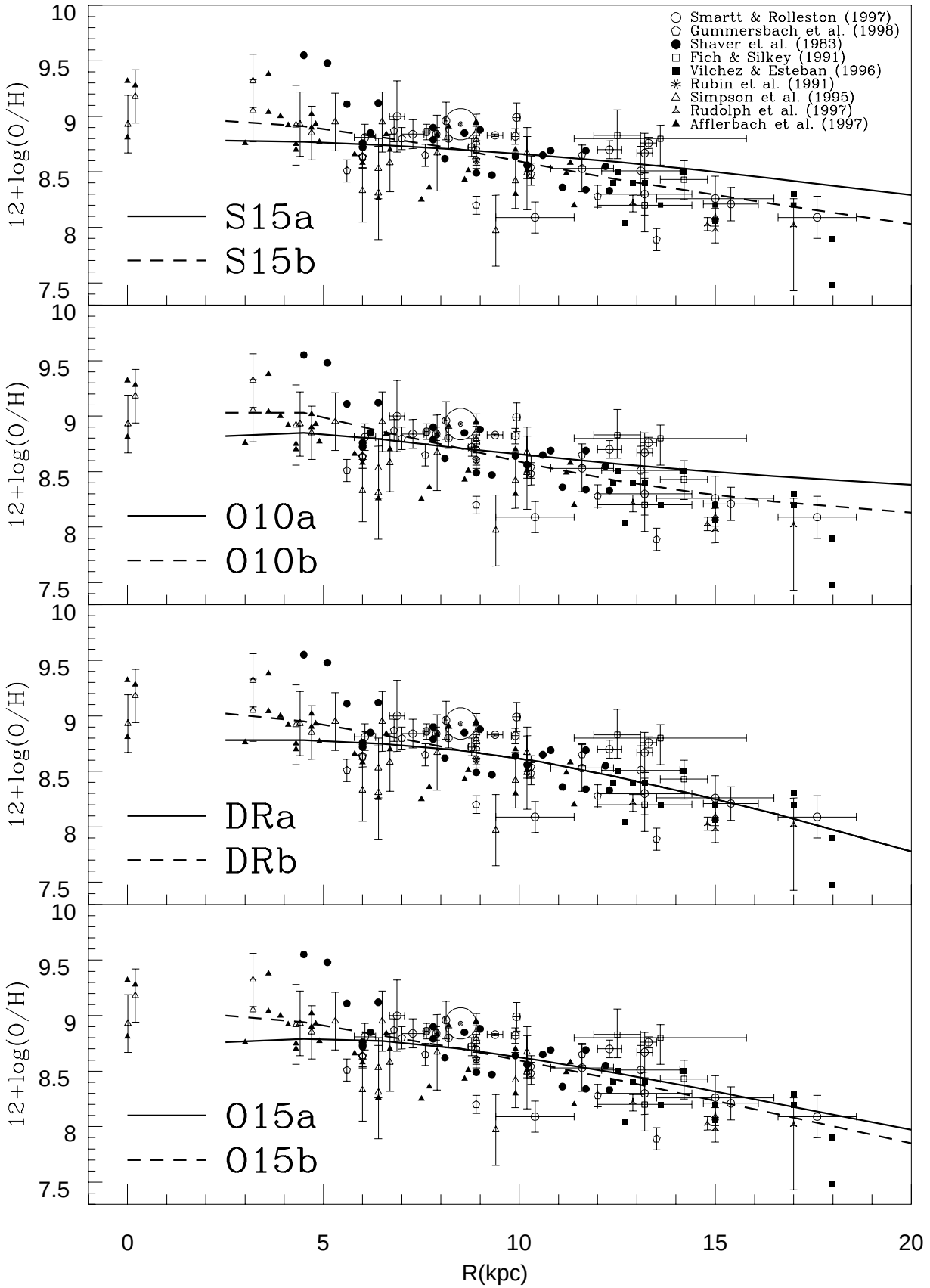

Fig. 1. Predicted radial oxygen gradient from the various models (see text) compared to observational data. The location of the Sun ⊙ is also displayed for comparison.

Table 2. Parameter values and resulting metallicity gradients of the models.

SF law	ν	ζ	r_d [kpc]	model	$\tau(r)$ [Gyr]		$\frac{d[O/H]}{dr}$ [dex kpc^{-1}]	
S15	0.35	0.2	4	S15a	3	(uniform)	–0.03	
				S15b	$3\,e^{\frac{r-r_\odot}{r_d}}$		–0.055	
					(from $\tau \sim 0.7$ at $r = 2.5$ to $\tau \sim 50$ at $r = 20$)			
O10	0.19	0.2	4	O10a	3	(uniform)	–0.03	
				O10b	$3\,e^{\frac{r-r_\odot}{r_d}}$		–0.06	
					(from $\tau \sim 0.7$ at $r = 2.5$ to $\tau \sim 50$ at $r = 20$)			
DR	0.45	0.2	4	DRa	3	(uniform)	–0.07	($r > r_\odot$)
							flat	($r < r_\odot$)
				DRb	3	($r \geq r_\odot$)	–0.07	
					$\sim 0.1 + \frac{r-2.5}{2}$	($r < r_\odot$)		
					(from $\tau \sim 0.1$ at $r = 2.5$ to $\tau = 3$ at $r \geq r_\odot$)			
				DRc	3	($r \geq 4.5$ kpc)	–0.06	
					$\sim 1 + (r - 2.5)$	($r < 4.5$ kpc)		
					(from $\tau \sim 1$ at $r = 2.5$ to $\tau = 3$ at $r \geq 4.5$)			
O15	0.35	0.2	4	O15a	3	(uniform)	-0.05	($r > r_\odot$)
							flat	($r < r_\odot$)
				O15b	$\sim 3\frac{r}{r_\odot}$		-0.065	
					(from $\tau \sim 1$ at $r = 2.5$ to $\tau \sim 7$ at $r = 20$)			
DRτ9	0.95	0.25	4	DRτ9a	9	(uniform)	–0.06	($r \gtrsim 12$ kpc)
							flat	($r \lesssim 12$ kpc)
				DRτ9b	$9\,e^{\frac{r-r_\odot}{3\ kpc}}$	($r \leq 10$ kpc)	–0.06	
					~ 50	($r > 10$ kpc)		
S15r_d35	0.35	0.2	3.5	S15r_d35a	3	(uniform)	–0.035	
				S15r_d35b	$3\,e^{\frac{r-r_\odot}{r_d}}$		–0.06	
					(from $\tau \sim 0.7$ at $r = 2.5$ to $\tau \sim 50$ at $r = 20$)			
O10r_d35	0.19	0.2	3.5	O10r_d35a	3	(uniform)	–0.03	
				O10r_d35b	$3\,e^{\frac{r-r_\odot}{r_d}}$		–0.06	
					(from $\tau \sim 0.7$ at $r = 2.5$ to $\tau \sim 50$ at $r = 20$)			
DRr_d35	0.45	0.2	3.5	DRr_d35a	3	(uniform)	–0.075	($r > r_\odot$)
							flat	($r < r_\odot$)
				Dr_d35Rb	3	($r \geq 6.5$)	–0.075	
					$\sim 1 + \frac{r-2.5}{2}$	($r < 6.5$)		
					(from $\tau \sim 0.1$ at $r = 2.5$ to $\tau = 3$ at $r \geq r_\odot$)			

the disc scale–length are discussed in Sect. 4.7 and Sect. 4.8. The adopted IMF is from Scalo (1986), uniform over the disc and constant in time, with an "amplitude" factor for SNæ Ia $A = 0.07$ (see Sect. 2.4 and PCB98 for further details). For each distinct SF law, the SF efficiency ν and the "IMF scaling fraction" ζ are calibrated so that at the Solar ring the model recovers the observed present-day surface gas density and oxygen abundance in the ISM (8–9 $M_\odot$ pc^{-2} and [O/H]$\sim$ 8.7 dex, respectively). With respect to the latter constraint, notice that the local ISM is oxygen-poor with respect to the Sun (e.g. Meyer et al. 1998, and Fig. 1), at odds with expectations from usual chemical models where metallicity always increases and

should be higher in the present-day ISM than in the Sun, formed about 5 Gyr ago. Different explanations have been put forward to account for this effect (dust depletion, orbital diffusion, SN II pollution at Sun formation, recent metal-poor infall...), but all of them are rather *ad hoc* or uneasy to model properly. Here we will not deal with this problem; following Prantzos & Aubert (1995) we just concentrate on the radial metallicity gradient, irrespectively of what the true zero-point abundance at the Solar ring actually is. Since the oxygen gradient is measured in young objects, we prefer to compare alike with alike and calibrate the model onto the ^{16}O abundance of the local ISM, rather than onto the solar one. Needless to say that models so calibrated will not reproduce the local age–metallicity relation and the solar metallicity; but the particular choice of the zero–point will not affect the radial behaviour of the models.

Once we have so fixed the same Solar point for all the models, we analyse the radial behaviour in the various cases. The calibrated values for ν and ζ for the various models presented are given in Table 2, together with model predictions for the oxygen gradient.

First of all we consider the constraint provided by the oxygen gradient as the best tracer of the overall metallicity (Wheeler et al. 1989), since it is the most abundant metal and the best sampled element in tracers of the present-day gradient (Sect. 3). Besides, its production and theoretical yields are the best understood of all the metals (Prantzos 1998), so the modelling of the abundance evolution of oxygen is quite reliable.

4.1. Models with Schmidt law (S15)

When a Schmidt law is adopted (Eq. 2 with $\kappa = 1.5$), if no radial variation of model parameters is assumed, the predicted gradient is far too flat (model S15a, Fig. 1). This is a well known result in literature (e.g. Lacey & Fall 1985; Edmunds & Greenhow 1995). Some further assumption is needed in models S15 to get a steeper oxygen gradient.

A typical prescription is to assume an "inside–out" formation scenario for the Galactic disc, namely that the infall timescale $\tau(r)$ is an increasing function of r (Chiosi & Matteucci 1980; Lacey & Fall 1983; Matteucci & François 1989). This can formally allow the model to predict a gradient close to the observed one (model S15b, Fig. 1), but the required variation of the infall timescale from the centre to the outskirts of the Galaxy is too large to be physically acceptable: in model S15b we need timescales much longer than the age of the Universe ($\tau \sim 50$ Gyr at $r = 20$ kpc, see Table 2). This would imply that the accretion process is still largely on-going; most of the Galaxy mass on the outskirts would be still accreting onto the disc nowadays. Such high accretion rates in spiral galaxies at the present day are not observed in the X-rays (Bertin & Lin 1996 and references therein), meaning that the accretion process should be mostly over by now.

We conclude that a simple Schmidt law is hardly suited at reproducing the observed metallicity gradients, at least within this kind of chemical models.

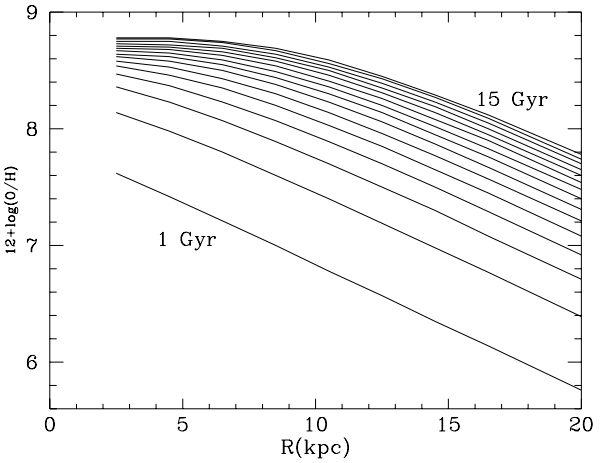

Fig. 2. Evolution of the oxygen gradient in model DRa. The gradient is plot at age steps of 1 Gyr, from 1 to 15 Gyrs.

4.2. Models with Oort–type SF law (O10)

In the case of the SF law by Oort (Eq. 3 with $\kappa = 1$), model O10a with a uniform infall timescale $\tau = 3$ Gyr still predicts too flat a metallicity gradient (Fig. 1). To recover the observed gradient in the inside–out formation scenario, as in the case of models S15 the required radial variation of τ becomes too extreme to be acceptable (model O10b, Table 2). This kind of SF law also proves unable to reproduce the observed oxygen gradient, at least within the framework of these chemical models.

4.3. Models with Dopita & Ryder's SF law (DR)

Model DRa is run with a uniform infall timescale τ=3 Gyr all over the disc. The predicted oxygen gradient is in good agreement with the data in the outer regions of the disc, while it flattens considerably in the inner regions (Fig. 1).

It is worth commenting a bit further on this effect. A linear gradient in [O/H]=12+log(O/H) implies an exponential decline of the metallicity Z. Therefore, a SF efficiency declining exponentially in radius, such as that by Dopita & Ryder, looks appealing to account for the metallicity gradient. In fact, simple closed models with such a SF law easily predict an exponential radial decrease of Z (Edmunds & Greenhow 1995). But in more realistic models this prediction falls, and the metallicity in the inner regions tends to settle onto some equilibrium value rather than follow the espected exponential profile. As noticed by various authors (Götz & Köppen 1992; Ferrini et al. 1994; Prantzos & Aubert 1995; Ryder 1995; Mollá et al. 1996, 1997), when infall is included and the IRA is relaxed, the model reaches a stage in which the metal enrichment provided by the ejecta of massive stars is significantly diluted by the primordial infalling gas and by the gas expelled by long–lived, low mass stars which formed at early times from relatively metal–poor gas. At this stage, metallicity abandons the one-to-one increase with SF processing and tends to settle on some equilibrium value. This effect is best seen in the inner regions of the Galaxy, where the SF process is more efficient: at the present age, most of the gas has

been eaten up already and SF has so much reduced as to be compensated by the gas shed by the many low-mass stars which had formed in the early, very active phases. As a consequence, in realistic models the radial metallicity profile tends to flatten in the inner regions. Fig. 2 shows how this effect develops in time: the gradient is linear (in [O/H]) at early ages, while for $t \gtrsim 5$ Gyr the metal enrichment slows down in the central parts due to the dilution effects of infall and of delayed return from low–mass stars.

Therefore, even in the case of an exponentially varying SF efficiency as in models DR, some further assumption is needed to steepen the abundance profile in the inner regions. In the inside–out formation scenario, we take the infall process to be faster in the inner regions, while in the outer regions ($r \geq r_\odot$) we can just keep a uniform $\tau = 3$ Gyr (model DRb, Fig. 1).

This kind of SF law, combined with an inside–out formation scenario, can reproduce the observed oxygen gradient within acceptable infall timescales over the whole disc.

4.4. An intermediate case: models O15

Though with an Oort–type SF law the preferred empirical exponent is suggested to be $\kappa = 1$ (Kennicutt 1998), some authors adopt $\kappa = 1.5$, which may be still compatible with Kennicutt's observations provided the whole disc model is considered altogether (Boissier & Prantzos 1999; Prantzos & Silk 1998). For the sake of completeness, we briefly discuss this SF law as well (Eq. 3 with $\kappa = 1.5$).

The behaviour of models O15 is qualitatively intermediate between models S15 or O10 and models DR (Fig. 1). Model O15a, adopting a uniform infall timescale $\tau = 3$ Gyr all over the disc, predicts a metallicity gradient which is steeper than in models S15a or O10a, but still shallower than the observed one, and shallower than in model DRa. The same flattening trend in the inner regions as in model DRa is also observed. With this SF law, model O15b is tuned to reproduce the observed gradient by means of a radial increase of the infall timescale τ, in the inside–out formation scenario (cfr. Table 2). At odds with model DRb, here $\tau(r)$ needs to increase over the whole radial range, otherwise the predicted gradient is not steep enough in the outer regions; but, unlike models S15b or O10b, one does not need to resort to unplausible timescales in the outskirts to recover the observed gradient.

Therefore, models O15 are acceptable toy–models (e.g. Prantzos & Silk 1998). We will not discuss them any further though, since we feel that an Oort–type SF law should be combined with the empirical exponent $\kappa = 1$ rather than 1.5 (Kennicutt 1998). In all what follows, the reader might simply keep in mind that models O15 would qualitatively display an intermediate behaviour between models S15/O10 and models DR.

4.5. Modelling the gradients of other elements

We have so far discussed the gradient of oxygen as the best tracer of the overall metallicity. With respect to the radial gradients of the other elements (Sect. 3), all the models presented above which reproduce the observed oxygen gradient (S15b, O10b, DRb) are also successful in predicting the other gradients (Fig. 3). This simply means that the adopted nucleosynthetic yields (from PCB98) are reliable. In fact, once a model is calibrated in ν, ζ and τ so as to give the right oxygen abundance and gradient, the predicted behaviour of other elements merely depends on the relative abundance ratios implied by the yields.

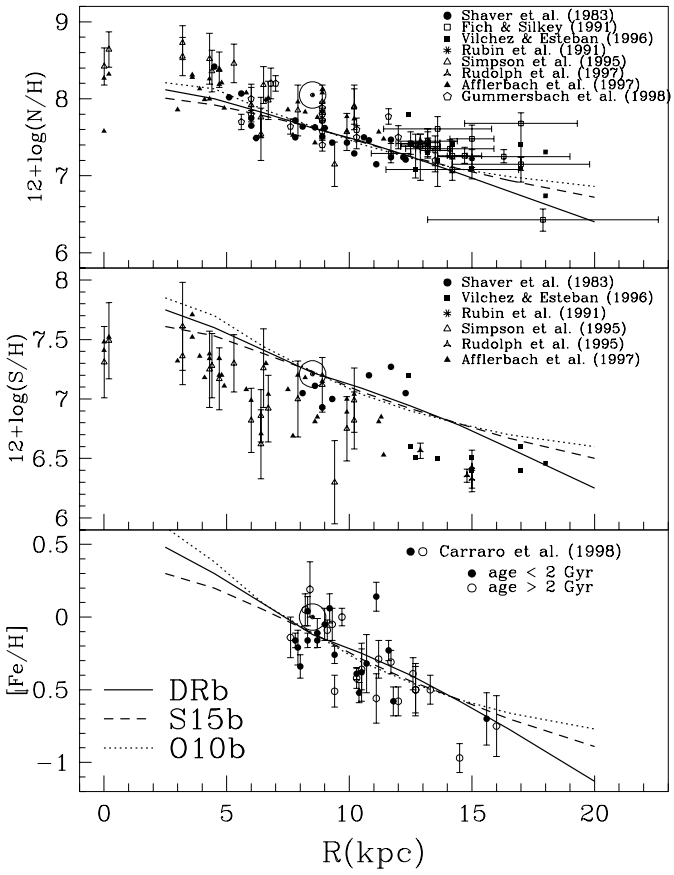

Fig. 3. Predicted nitrogen, sulfur and iron gradients from models indicated in the legend on bottom left (see text) compared to observational data.

Fig. 3 just shows some problem with the zero-point of the sulfur gradient (middle panel): the slope of the gradient is correct but the overall abundance is too high. This can be ascribed to the uncertainties in the yields of ^{32}S from SNæ II. The mismatch between the predicted and observed sulfur abundance goes here in the opposite direction with respect to evidence from stars in the Solar Neighbourhood, which rather indicates that theoretical yields for ^{32}S are too low (PCB98). But the data on the ^{32}S abundance in low-metallicity local stars are quite few and old; further and improved observational data are needed to shed light on the problem of the yields of ^{32}S.

On the base of the constraint provided by the metallicity gradient, we can consider DR as viable models, while we tend to exclude models S15 and O10, and the corresponding SF laws, since they would require unacceptably long accretion timescales in the outskirts of the Galaxy. The situation may though change

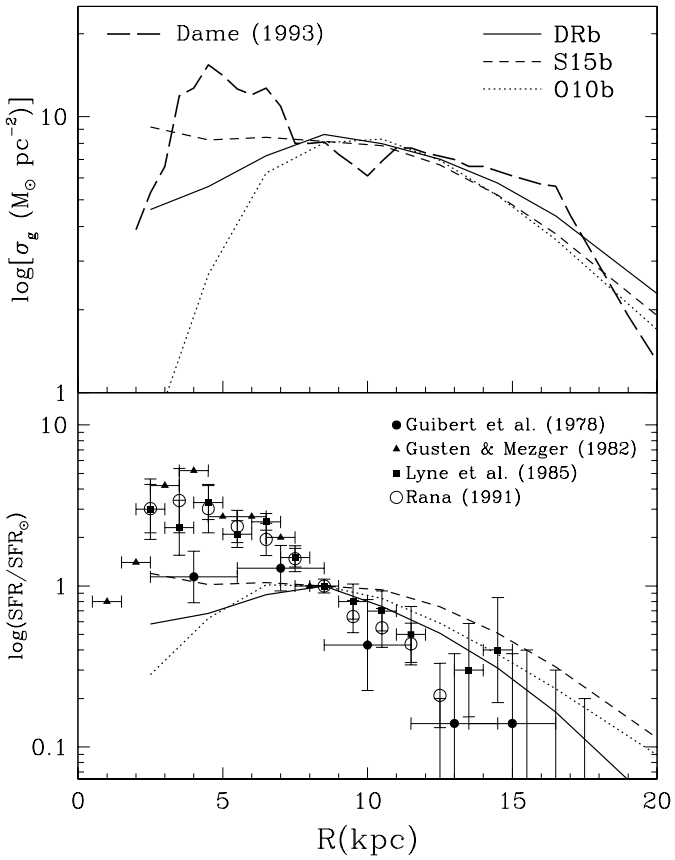

Fig. 4. Observed radial gas and (normalized) SFR distribution, together with predictions from the models in the legend on top right.

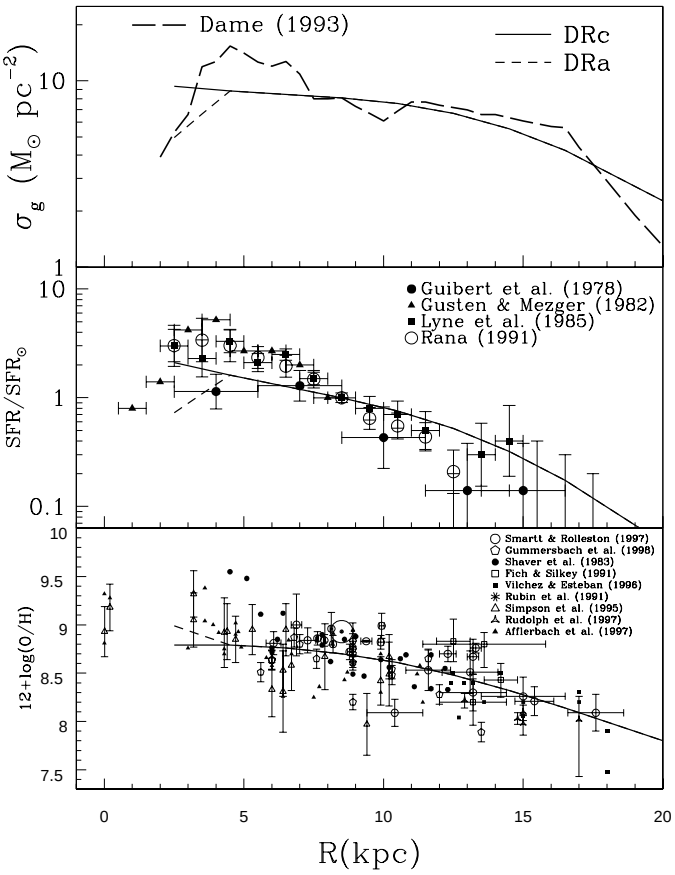

Fig. 5. Model DRc, tuned so as to predict a maximum in the gas distribution around 4–5 kpc, still cannot reproduce the observed peak (see text)

if radial inflows of gas are allowed for (e.g. Lacey & Fall 1985; Götz & Köppen 1992; Portinari & Chiosi 1999).

4.6. Modelling the gas and SF profiles

All of the models which are tuned, with more or less plausible model parameters, to give successful predictions for the metallicity gradient (S15b, O10b, DRb) fall short at reproducing the observed radial profiles of gas density and SFR (Fig. 4). In particular, they cannot account for the peak in the gas density corresponding to the molecular ring around 4 kpc, and the corresponding peak in SF activity. Model S15 also seems to predict too high a SFR outward of the Solar ring, in agreement with the remark by Prantzos & Silk (1998) that the present–day SFR along the disc does not resemble any simple power law of the gas density. This latter feature favours, in general, SF laws with a radially varying efficiency (as in models DRb and O10b) with respect to simple Schmidt laws.

In models S15b, O10b, DRb the radial dependence of the infall timescale was tuned so as to optimize the slope of the predicted metallicity gradient (Fig. 1); these models tend to yield a maximum in the gas distribution around $r_\odot$ (Fig. 4). One can also adjust the infall timescale so as to shift the maximum in gas density and SFR around 4–5 kpc, while keeping somewhat compatible with the observed metallicity gradient (e.g. model DRc in Fig. 5); still, the sharp peak of the molecular ring is never recovered (see also Prantzos & Silk 1998).

It seems to be impossible for these models to reproduce both the metallicity gradient and the radial gas distribution at the same time. This is easily interpreted in the framework of "static" chemical models, or models consisting of isolated rings, like ours. To produce a higher metallicity in the inner regions, SF must have been more effective there, and consequently the available gas must have been more efficiently processed, consumed and locked in long-lived stars or remnants. In the models, the present–day gas density decreases where the metallicity is higher, at odds with observations.

A possible way out, in the framework of simple static models, might be to assume that the IMF is skewed toward high masses in the inner regions (higher ζ or flatter power–law exponent). A higher percentage of massive stars provides in fact a more efficient chemical enrichment, while less gas remains locked in low–mass stars and the gas density can keep high. But the issue of systematic variations in the IMF is still very controversial, both on empirical and on theoretical grounds (Scalo 1998a,b).

A less "exotic" possiblity than a strongly varying IMF along the disc is that the formation of the molecular ring involves some kinematical or dynamical process, not accounted for in

simple static chemical models. As is the case for rings in outer barred spirals, it is likely that the molecular ring in our Galaxy has formed because of gas accumulation at the Lindblad resonances of a barred potential. Models for the Galactic bar set its co–rotation between 2.5 and 3.5 kpc, and its Outer Lindblad Resonance between 4.5 and 6 kpc (e.g. Gerhard 1996 and references therein), which suggests a correlation between the molecular ring and the dynamical effects of the bar. In order to reproduce these effects, chemical models should allow for Bar–induced radial drifts of gas. Hereon the need to develop chemical models with radial flows of gas, which will be the subject of a second paper (Portinari & Chiosi 1999).

4.7. The effects of a longer infall timescale

All the models presented so far adopt an infall timescale of 3 Gyr at the Solar ring, as the fixed point for the radial variation of τ in the inside–out formation scenario. The accretion timescale for open chemical models of the Solar Neighbourhood is usually fixed by the metallicity distribution of local G–dwarfs. For many years, the reference dataset was that by Pagel & Patchett (1975), later revised by Pagel (1989) and by Sommer–Larsen (1991a). This distribution was nicely fitted with infall timescales of 3–4 Gyr (e.g. Chiosi 1980; Matteucci & François 1989; Sommer–Larsen 1991a).

The latest datasets by Wyse & Gilmore (1995) and Rocha–Pinto & Maciel (1996) display a narrower distribution of the stars in metallicity, with a prominent peak around [Fe/H]~ -0.2, and therefore favour much longer accretion timescales, up to 8–9 Gyr (Chiappini et al. 1997; PCB98). Such timescales may be uncomfortably long from the dynamical point of view: in dynamical simulations the gas tends to settle onto the equatorial plane within the first 3–6 Gyrs (e.g. Burkert et al. 1992; Sommer-Larsen 1991b; although Samland et al. 1997 suggest longer disc formation timescales).

Even more problematic here, if the adopted infall timescale is so long, it is hard for the chemical model to reproduce the observed metallicity gradient. Let's consider, among the various SF laws studied here, the one which intrinsically gives the steepest metallicity gradient, namely Dopita & Ryder's law. Model DRτ9a adopts a uniform infall timescale $\tau = 9$ Gyr, rather than 3 Gyr (Table 2). The resulting metallicity gradient is quite shallow (Fig. 6, solid line), much shallower than the gradient predicted by the analogous model DRa with $\tau = 3$ Gyr (dotted line). In fact, when the infall timescale is very long, the dilution effect (Sect. 4.3) is stronger and an equilibrium value for metallicity is reached over a larger range of radii, leading to an overall flat gradient. To reproduce the observed gradient within the inside–out scenario (model DRτ9b, dashed line) the assumed infall timescale for $r \gtrsim 10$ kpc needs to be of $\sim$50 Gyr (Table 2), implying too large infall rates at the present day. With other SF laws, things get even worse.

Radial inflows of gas in the disc can improve on this point, since they both affect the predicted G–dwarf distribution contributing to solve the G–dwarf problem, and favour the formation of the metallicity gradient (Lacey & Fall 1985; Clarke 1991; Götz & Köppen 1992). This will be discussed in more detail in a forthcoming paper (Portinari et al. 1999, in preparation).

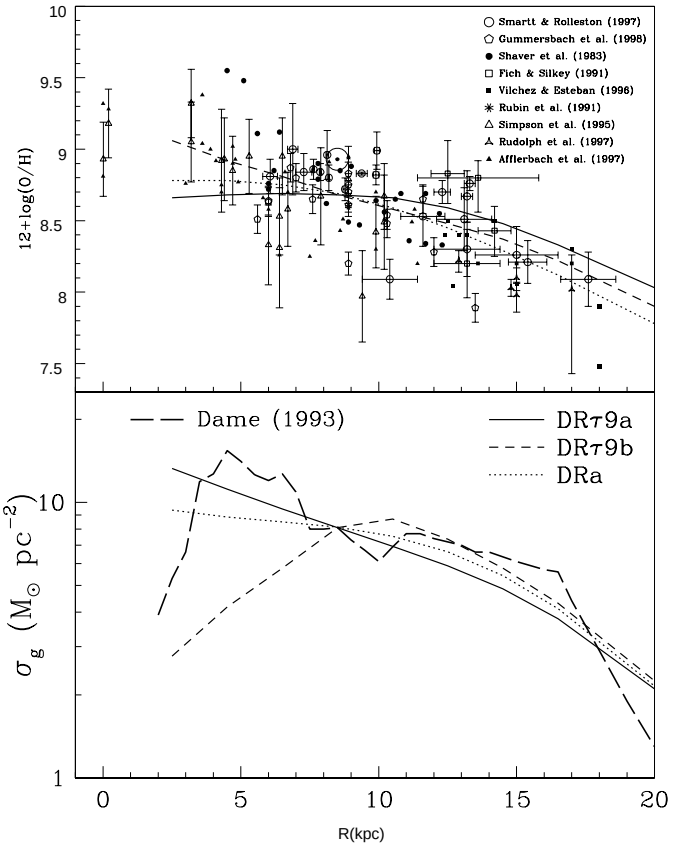

Fig. 6. Predicted oxygen gradient and gas distribution from model DRτ9a adopting a uniform infall timescale $\tau = 9$ Gyr (solid line), compared to model DRa adopting $\tau = 3$ Gyr (dotted line) and to the observational data. Model DRτ9b, adopting $\tau = 9$ Gyr at the Solar ring, is calibrated with τ increasing with radius so as to reproduce the observed gradient (see text).

Finally, Fig. 6 shows how it is still impossible to reproduce at the same time the metallicity gradient and the gas peak around 4 kpc, also with models DRτ9a,b. Namely, the conclusions drawn in Sect. 4.6 remain valid irrespectively of the adopted $\tau(r_\odot)$.

4.8. The effects of a shorter disc scale–length

All the models presented so far adopt an exponential scale length for mass density $r_d = 4$ kpc, quite typical of chemical evolution models (e.g. Sommer–Larsen 1991b, Köppen 1994, Rana 1991) and consistent with early determination of the optical scale length of the Galactic disc (e.g. Binney & Tremaine 1987 and references therein; Kuijken & Gilmore 1989). Recent observations, however, tend to suggest a shorter scale length for disc stars, $\lesssim 3$ kpc (Sackett 1997 and references therein, Vallenari et al. 1999 and references therein), comparable to that of other Sbc galaxies. With $r_d = 4$ kpc, our chemical models yield a final (present-day) *stellar* density profile with scale length between 3 and 3.5 kpc (Fig. 7, top panel), still compatible but somewhat

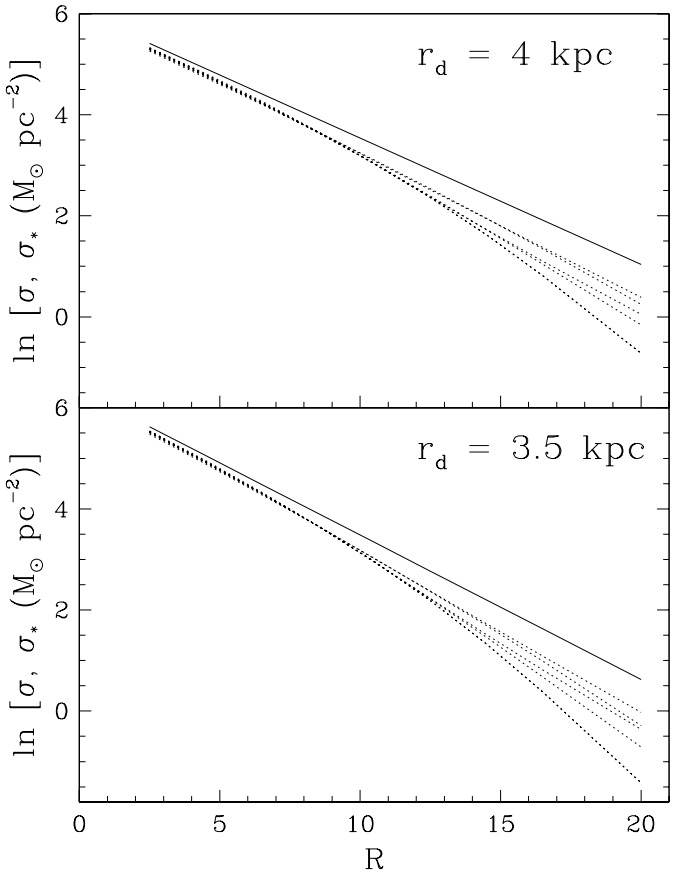

Fig. 7. *Top panel*: surface mass density profile (solid line) and corresponding stellar density profile (dotted lines) for models with r_d = 4 kpc. *Bottom panel*: the same plot for models with $r_d = 3.5$ kpc.

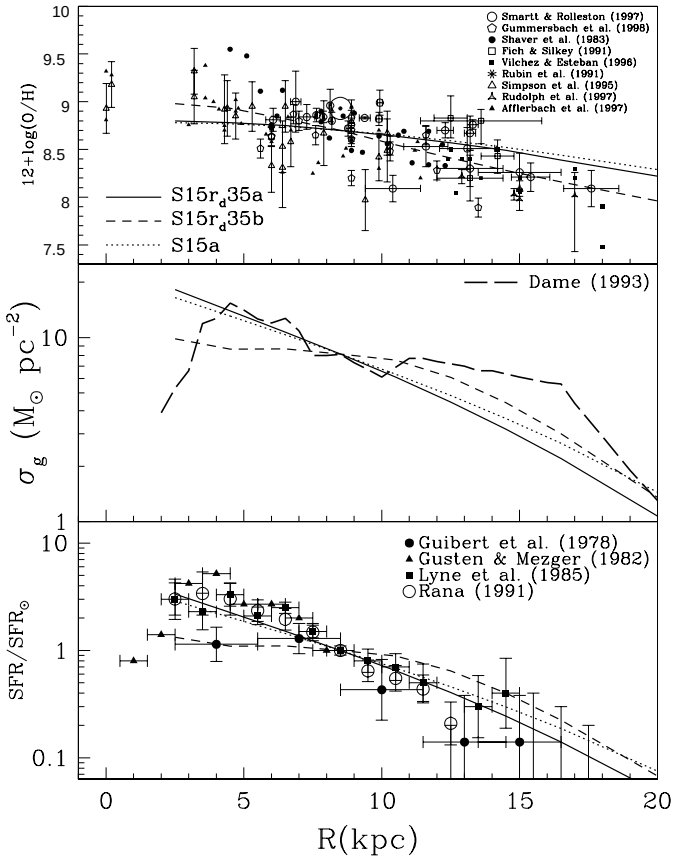

Fig. 8. Predicted oxygen gradient and gas and SFR profiles from model S15r_d35a adopting a disc scale length $r_d = 3.5$ kpc (solid line), compared to model S15a adopting $r_d = 3.5$ kpc (dotted line) and to the observational data. Model S15r_d35b is calibrated with τ increasing with radius so as to reproduce the observed gradient (see text).

long with respect to the latest observations. Therefore, in this section we explore models with a shorter mass density scale-length, $r_d = 3.5$ kpc, corresponding to a final stellar density scale length around 2.5–3 kpc (Fig. 7, bottom panel).

Models S15r_d35a, O10r_d35a and DRr_d35a correspond exactly to models S15a, O10a and DRa respectively, a part from the adopted scale length (see Table 2). The shorter scale length tends to favour the formation of the metallicity gradient and to predict a bit steeper decline of the gas density in the outer parts (compare solid to dotted lines in Fig. 8 to 10). The effect is though minor on models S15 and O10, so that extreme infall timescales still need to be invoked to reproduce the metallicity gradient in the inside–out scenario (models S15r_d35b and O10r_d35b in Figs. 8 and 9; see also Table 2). The effect of the steeper disc profile is more evident in models DR, where the SF efficiency scales directly with surface density (Sect. 2.3); nontheless, to reproduce the observed metallicity gradient shorter infall timescales need to be assumed in the inner regions, in accordance with the inside–out scenario. The problem of reproducing the molecular ring is still present as well.

In the overall, adopting a shorter scale–length (within observational limits) does not influence the bulk of the conclusions we drew in the previous sections.

5. Summary and conclusion

From our analysis of chemical models for the Galactic disc with different SF laws, it is evident that none of the SF laws considered is able, by itself, to reproduce the observed metallicity gradient throughout the whole extent of the disc. Some further "dynamical" assumption is needed in any case, such as an inside–out formation scenario (Larson 1976; Chiosi & Matteucci 1980; Lacey & Fall 1983; Matteucci & François 1989).

Even SF laws with an exponentially decreasing efficiency (e.g. Dopita & Ryder's law), which in simple closed models would predict a logarithmic metallicity gradient like the observed one, display a more complex behaviour in detailed open models with no IRA. In particular, due to the late dilution of the enriched ejecta of massive stars with infalling gas and returned gas from long-lived stars, the metallicity gradient tends to flatten in the inner regions with respect to the outer slope. To recover the observed slope, infall timescales need to be shorter in the inner regions, to reduce the effects of dilution at late times. This shows how relaxing the IRA has non-negligible effects on chemical models, even in the case of oxygen which is produced on very short timescales and for which it is often assumed that neglection of finite stellar lifetimes is a viable approximation.

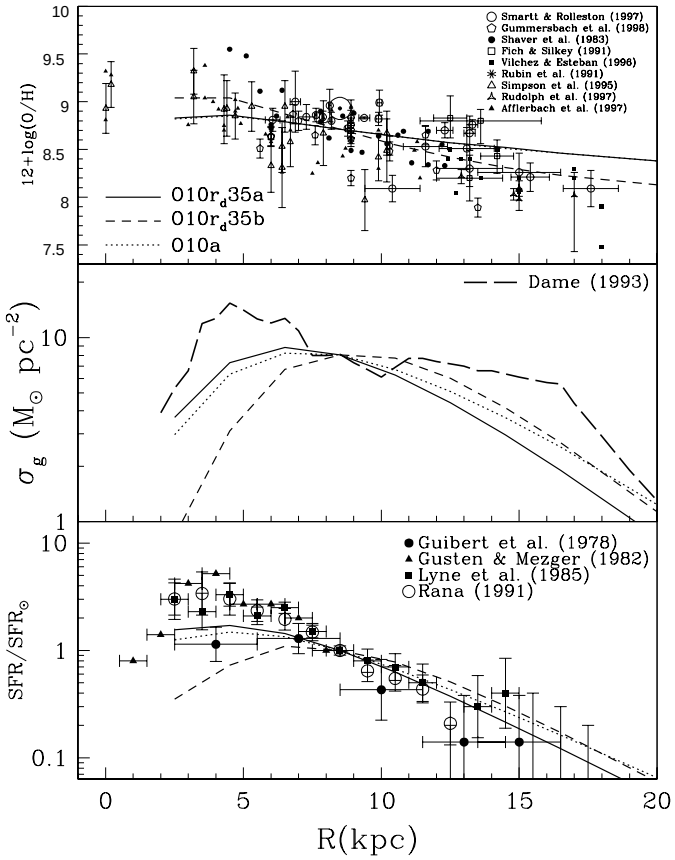

Fig. 9. Same as Fig. 8, but for models O10.

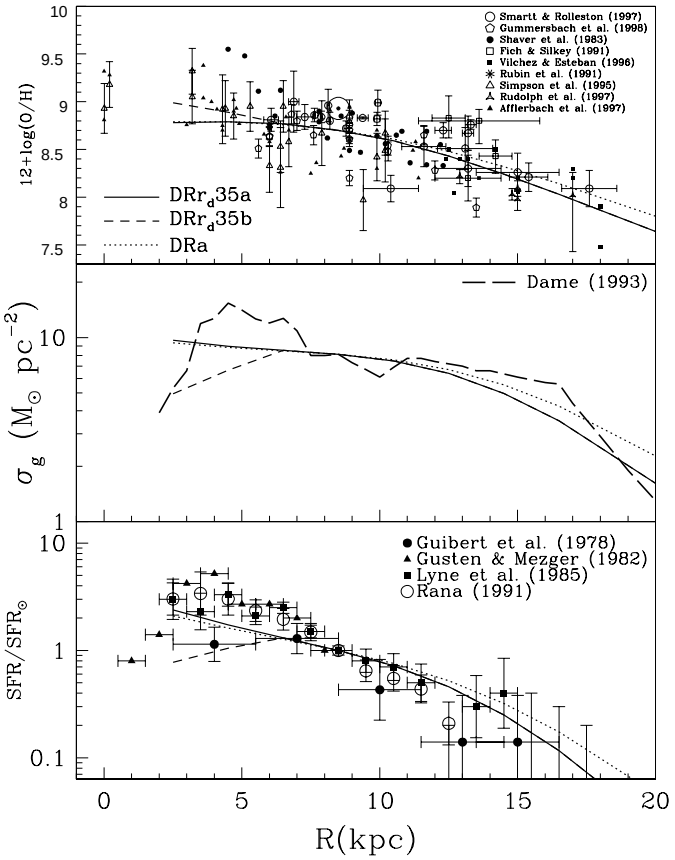

Fig. 10. Same as Fig. 8 and 9, but for models DR.

Though this might hold for the massive stars producing oxygen itself, the gas shed on delayed return from low-mass stars ultimately affects also the evolution of the oxygen abundance.

A Schmidt SF law with $\kappa = 1.5$ or an Oort–type SF law with $\kappa = 1.0$, though nicely fitting some empirical relations (Kennicutt 1998), are unable to account for the observed metallicity gradients even in the inside–out picture, because the required radial variation of the infall timescale $\tau(r)$ implies accretion timescales in the outer regions much longer than a Hubble time. These SF laws are therefore excluded, within the framework of simple "static" chemical models. These conclusions may change in the presence of radial flows of gas (Portinari & Chiosi 1999).

We verified that these results are valid in general, irrespectively on the adopted scale length of disc surface density (at least within observational estimates) and on the adopted infall timescale at the Solar ring. If the latter is very long, as maybe suggested from recent results on the "G–dwarf problem", even SF laws of the Dopita & Ryder type hardly reproduce the metallicity gradient within the inside–out scenario.

Finally, with these "static" chemical models it turns out to be very difficult to reproduce at the same time both the metallicity gradient and the gas distribution, in particular the molecular ring (unless one resorts to exotic possibilities like a varying IMF along the disc). Since the molecular ring is likely to be due to the dynamical influence of the Galactic bar, chemical models allowing for radial drifts and accumulation of gas might be needed to mimick these effects and reproduce the corrects gas distribution. Our next step will be to improve the chemical model including radial flows of gas (Portinari & Chiosi 1999).

Acknowledgements. We thank Yuen K. Ng, Antonella Vallenari, Fulvio Buonomo and Giovanni Carraro for useful discussions on Galactic structure and dynamics, and the referee whose comments improved the presentation of our paper. L.P. acknowledges kind hospitality from the Nordita Institute in Copenhagen, from the Observatory of Helsinki and from Sissa/Isas in Trieste. This study has been financed by the Italian Ministry for University and for Scientific and Technological Research (MURST) through a PhD fellowship and the contract "Formazione ed evoluzione delle galassie", n. 9802192401.

References

Afflerbach A., Churchwell E., Werner M.W., 1997, ApJ 478, 190
Bertin G., Lin C.C., 1996, Spiral structure in galaxies – A density wave theory. MIT Press, Cambridge, Massachusetts
Binney J., Tremaine S., 1987, Galactic dynamics. Princeton University Press
Boissier S., Prantzos N., 1999, MNRAS 307, 857
Bressan A., Chiosi C., Fagotto F., 1994, ApJS 94, 63
Burkert A., Truran J.W., Hensler G., 1992, ApJ 391, 651
Carraro G., Ng Y.K., Portinari L., 1998, MNRAS 296, 1045
Chiappini C., Matteucci F., Gratton R.G., 1997, ApJ 477, 765
Chiosi C., 1980, A&A 83, 206

Chiosi C., Matteucci F., 1980, Mem. Soc. Astron. Ital. 51, 107
Chiosi C., Matteucci F., 1982, A&A 105, 140
Clarke C.J., 1991, MNRAS 249, 704
Dame T.M., 1993, In: Holt S., Verter F. (eds.) Back to the Galaxy. p. 267
Dopita M.A., 1985, ApJ 295, L5
Dopita M.A., Ryder S.D., 1994, ApJ 430, 163
Edmunds M.G., Greenhow R.M., 1995, MNRAS 272, 241
Ferrini F., Mollá M., Pardi M.C., Díaz A.I., 1994, ApJ 427, 745
Fich M., Silkey M., 1991, ApJ 366, 107
Fitzsimmons A., Brown P.J.F., Dufton P.L., Lennon D.J., 1990, A&A 232, 437
Fitzsimmons A., Dufton P.L., Rolleston W.R.J., 1992, MNRAS 259, 489
Friel E.D., 1995, ARA&A 33, 381
Gehren T., Nissen P.E., Kudritzki R.P., Butler K., 1985, In: Production and distribution of CNO elements. Proceedings of ESO workshop, p. 171
Gerhard O.E., 1996, IAU Symp. 169, 79
Götz M., Köppen J., 1992, A&A 262, 455
Guibert J., Lequeux J., Viallefond F., 1978, A&A 68, 1
Gummersbach C.A., Kaufer A., Schäfer D.R., Szeifert T., Wolf B., 1998, A&A 338, 881
Güsten R., Mezger M., 1982, Vistas in Astron. 26, 159
Janes K.A., 1979, ApJS 39, 135
Kaufer A., Szeifert Th., Krenzin R., Baschek B., Wolf B., 1994, A&A 289, 740
Kennicutt R.C., 1998, ApJ 498, 541
Kilian-Montenbruck J., Gehren T., Nissen P.E., 1994, A&A 291, 757
Köppen J., 1994, A&A 281, 26
Kuijken K., Gilmore G., 1989, MNRAS 239, 571
Lacey C.G., Fall M., 1983, MNRAS 204, 791
Lacey C.G., Fall M., 1985, ApJ 290, 154
Larson R.B., 1976, MNRAS 176, 31
Lynden–Bell D., 1975, Vistas in Astron. 19, 229
Lyne A.G., Manchester R.N., Taylor J.H., 1985, MNRAS 213, 613
Maciel W.J., Köppen J., 1994, A&A 282, 436
Matteucci F., François P., 1989, MNRAS 239, 885
Meyer D., Jura M., Cardelli J.A., 1998, ApJ 493, 222
Mollá M., Ferrini F., Díaz A.I., 1996, ApJ 466, 668
Mollá M., Ferrini F., Díaz A.I., 1997, ApJ 475, 519
Oort J.H., 1974, IAU Symp. 58, 375
Pagel B.E.J., 1989, In: Beckman J.E., Pagel B.E.J. (eds.) Evolutionary phenomenta in galaxies. Cambridge University Press, p. 201
Pagel B.E.J., Patchett B.E., 1975, MNRAS 172, 13
Portinari L., Chiosi C., Bressan A., 1998, A&A 334, 505 (PCB98)
Portinari L., Chiosi C., 1999, A&A, submitted
Prantzos N., 1998, In: Abundance profiles: diagnostic tools for galaxy history. ASP Conf. Ser. 147, 171
Prantzos N., Aubert O., 1995, A&A 302, 69
Prantzos N., Silk J., 1998, ApJ 507, 229
Rana N.C., 1991, ARA&A 29, 129
Roberts W., 1969, ApJ 158, 123
Rocha–Pinto H.J., Maciel W.J., 1996, MNRAS 279, 447
Rubin R.H., Simpson J.P., Haas M.R., Erickson E.F., 1991, ApJ 374, 564
Rudolph A.L., Simpson J.P., Haas M.R., Erickson E.F., Fich M., 1997, ApJ 489, 94
Ryder S.D., 1995, ApJ 444, 610
Sackett P., 1997, ApJ 483, 103
Saio H., Yoshii Y., 1990, ApJ 363, 40
Samland M., Hensler G., Theis C., 1997, ApJ 476, 544
Salpeter E., 1955, ApJ 121, 161
Scalo J.M., 1986, Fund. Cosmic Phys. 11, 3
Scalo J.M., 1998a, In: The Stellar Initial Mass Function. ASP Conf. Ser. 142, 201
Scalo J.M., 1998b, Proceedings for: The Birth of Galaxies. Blois, France, June 1998, (astro–ph 9811341)
Schmidt M., 1959, ApJ 129, 243
Shaver P.A., McGee R.X., Newton M.P., Danks A.C., Pottasch S.R., 1983, MNRAS 204, 53
Shu F., Milione V., Gebel W., et al., 1972, ApJ 173, 557
Simpson J.P., Colgan S.W.J., Rubin R.H., Erickson E.F., Hass M.R., 1995, ApJ 444, 721
Smartt S.J., Rolleston W.R.J., 1997, ApJ 481, L47
Sommer-Larsen J., 1991a, MNRAS 249, 368
Sommer-Larsen J., 1991b, MNRAS 250, 356
Talbot R.J., Arnett D.W., 1975, ApJ 197, 551
Vallenari A., Bertelli G., Schmidtobreick L., 1999, to be submitted
Vilchez J.M., Esteban C., 1996, MNRAS 280, 720
Wang B., Silk J., 1994, ApJ 427, 759
Wheeler J.C., Sneden C., Truran J.W., 1989, ARA&A 27, 289
Wyse R.F.G., Gilmore G., 1995, AJ 110, 2771
Wyse R.F.G., Silk J., 1989, ApJ 339, 700